Detecting Scalable Obstacles Using Soft Sensors in the Body of a Compliant Quadruped

Doğa Özbek, Talip Batuhan Yılmaz, Mert Ali İhsan Kalın, Kutay Şentürk, and Onur Özcan

***Abstract*—In soft robotics, one of the trending topics is using soft sensors to have feedback from the robot's body. This is not an easy process to accomplish since the sensors are often nonlinear, so researchers use different methods to generate information from data such as filters, machine learning algorithms, and optimization algorithms. In this paper, we show that, with good electronic and mechanical design, it is possible to use soft sensors for detecting obstacles and distinguishing the scalable obstacles. The demonstration is conducted with an untethered miniature, soft, C-legged robot, M–SQuad, the first modular C-legged quadruped consisting of three modules, which are connected by four soft sensors. In M–SQuad's body design, sensors are utilized as both sensing and structural elements. The modular design of the M–SQuad allows testing different sensor geometries and replacing the malfunctioning parts easily, without the need to refabricate the entire robot. A case study is introduced for demonstration of the robot's capability of detecting obstacles and distinguishing scalable obstacles in a parkour consisting of two obstacles with the heights of 20 mm and 150 mm, respectively. In the case study, M–SQuad can detect an obstacle during locomotion using the coil-spring shaped soft sensors in its body. Moreover, it can distinguish the obstacle is scalable or not after an initial climbing trial. If the obstacle is not scalable, the robot turns back.**

***Index Terms*—Legged robots, soft robot materials and design, soft sensors.**

I. Introduction

IN MINIATURE soft robotics, one of the significant points to focus on is using body undulations or deformations for the environmental perception such as obstacle detection, inclined plane detection or shape recognition of obstacles, similar to how biological organisms function. Soft robots or soft mechanisms may have ability to use soft sensors embedded to their bodies, legs, or feet for environmental state feedback. Soft robots are more complex to control than the rigid robots due to the high degree of freedom due to their soft nature [1], hence they require the use of many sensors or rely on external control inputs to achieve simple tasks. Thus, if soft sensors can be used for feedback, rigid sensors can be replaced with soft sensors in most of the soft mechanisms, which can be a milestone to have fully soft robots in the future.

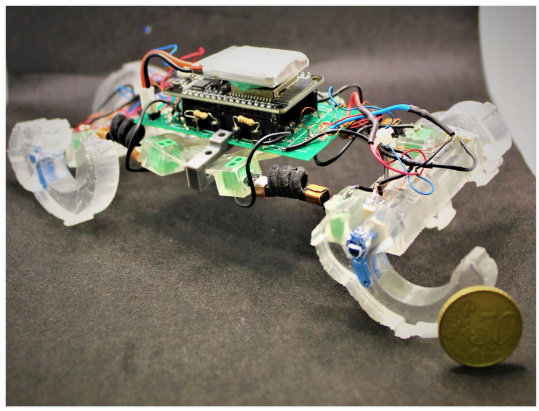

Fig. 1. Modular soft quadruped (M–SQuad).

In addition, observing the details of biology is an essential point, because understanding how the biological structures work provides inspiration to the soft robot mechanisms [2], [3]. Worm-like soft robots have their principle of locomotion from biology and nature. They can move by simple mechanical actuations such as extension, torsion and bending supplied by hydraulic actuators [4]. Pneumatic actuators are also often used in soft robotics, especially for gripper mechanisms [5], which are actuated like biological muscles [6], [7]. For normal size to large scale mobile robots, it is beneficial to use hydraulic or pneumatic actuation systems. On the other hand, using pneumatic or hydraulic actuators hinder the possibility for miniaturization of robot designs due to the need to carry pumps or pressurized canisters. To solve the miniaturization problem, the soft miniature quadruped SEAQ is actuated by shape memory alloys [7]. In our work, we preferred micro brushed motors for the actuation of the C-legs to make M–SQuad walk. A picture of our modular soft quadruped M-SQuad is shown in Fig. 1.

To provide environmental perception, robots often utilize rigid sensors. However, when used in soft robots, these rigid sensors limit soft robots' full potential by making them stiffer. Rigid obstacle detection sensors, apart from lidars, also do not offer the range of which soft stretchable sensors could provide. As a result, there are only a few examples of autonomous and fully soft robots [8]. To overcome this problem and to increase

Manuscript received October 11, 2021; accepted December 23, 2021. Date of publication January 10, 2022; date of current version January 20, 2022. This letter was recommended for publication by Associate Editor Je-Sung Koh and Editor Kyu-Jin Cho upon evaluation of the reviewers' comments. This work was supported by the Scientific and Technological Research Council of Turkey (TUBITAK) under Grant 216M195. *(Corresponding author: Onur Ozcan.)*

The authors are with the Department of Mechanical Engineering, Bilkent University, 06800 Ankara, Turkey (e-mail: doga.ozbek@bilkent.edu.tr; talipbatuhan yilmaz@gmail.com; aliihsankalin@gmail.com; kutaysenturk12@gmail.com; onurozcan@bilkent.edu.tr).

The video shows the resistance change vs. deformation experiment for the soft sensor. Additionally, M-SQuad with scalable and non-scalable obstacles are shown together with sensor data. Finally a demonstration of the robot distinguishing obstacle scalability is presented.

Digital Object Identifier 10.1109/LRA.2022.3141655

soft robots' ability to perceive their surroundings, there have been continuous research being conducted in the field of soft sensors [9]–[11]. In the literature, there are soft robots that use biosensing to perceive their environment [12]. For wearable robots, soft sensors can be used to assess human gaits [13], [14]. There are also examples of soft electronic skins, however, most are not yet used on mobile robots [15]. A flexible piezoelectric sensor array embedded into the feet of a legged robot for terrain recognition is another example of a soft sensor application for a walking robot. [16]. However, soft sensors are often highly nonlinear, which affects the quality, reliability and repeatability of the data acquired. To eliminate nonlinearity issues, machine learning models are developed [17]. However, in our study, we used the raw data acquired from the sensor because determining if the obstacle is scalable is possible by measuring the elapsed time for which the sensor response stays saturated during the climbing process.

In this study, our main aim is to improve our soft miniature C-shaped legged quadruped, SQuad, previously presented in [18], by giving it the ability to recognize if an obstacle is scalable. To achieve this, we have modified SQuad and divided it into 3 modules: back, middle and front. The new design is similar to the modular robot design shown in [19], however the modules of M–SQuad are connected to each other using four 3D printed soft sensors, rather than passive PDMS pieces. In literature, the fabrication of soft sensors is mostly done using PMDS impregnated with conductive carbon particles (cPDMS) [6]. Our sensors are printed with an FDM 3D printer using the conductive Eel filament of NinjaTek. With the addition of the soft sensors, the modified SQuad is now able to assess the obstacle to decide to whether cancel the climbing process or to commit climbing. This sensing protects the robot from attempting a dangerous maneuver and prevents it from tipping over and becoming inoperative.

The main contributions of this paper are the design and integration steps of 3D printed soft sensors into a soft quadruped robot, and using the soft sensors to decide the scalability of the obstacles. Our experiments demonstrate that coil-spring shape sensors are successful in terms of detecting the obstacles because of the significant resistance change the sensors experience when bent until the two adjacent coils touch. In addition, the modular design of the M–SQuad, and the use of sensors as both structural and sensing elements are novel design aspects for miniature soft robotics. If a problem occurs on any module of the M–SQuad, it can be changed or replaced, without repeating all the molding processes for the entire body; only the problematic module can be replaced without changing the other modules. The sensors can also be changed or replaced if a problem occurs on any sensors, or if a different geometry sensor will be utilized.

II. Design of Modular SQuad

A. Body Design

The main inspiration behind the M–SQuad's body design is to soften the sensorized parts of the robot body to maximize the bending amount the soft sensors experience during locomotion. On the other hand, we don't want the robot's body touching down during locomotion in order to avoid unnecessary forces caused by dragging. As a result, we ended up designing a more rigid motor mounting part and a middle electronics carrier module, but softer module connecting sensors, compared to M-SQuad's brother SQuad [18].

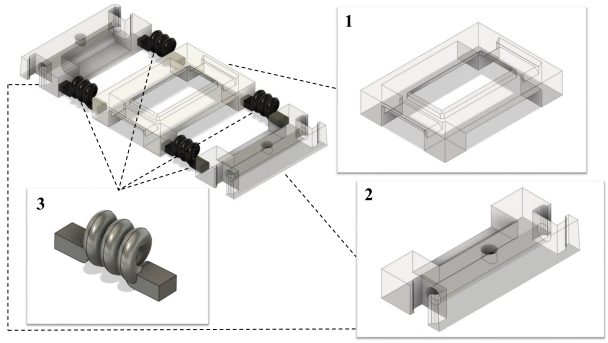

Fig. 2. CAD drawing of the body of the M–SQuad together with sensors. (1) Main module (2) Motor end module (3) Soft sensors.

The M–SQuad's body design consists of three modules, which can be listed as: back module, middle module and front module. The front and back modules are identical modules. Since they carry the motors, they are both called motor end modules. The middle part is designed to carry PCB and battery, all the wires are distributed from this module to motor end modules. Thus, this module is called the main module. The motor end modules are mechanically connected to the main module via two soft sensors. A schematic of the robot's body is shown in Fig. 2.

In order to provide necessary electrical connections between the sensors and the microcontroller, double row PCB screw terminals are used. Four of these screw terminals are embedded to middle module and two screw terminals are embedded to each motor end module during the curing of the PDMS in the module molding step. Sensor connections are prepared with respect to this double row PCB screw terminals which have dimensions of 5 mm x 5 mm x 6 mm. The used screw-in terminals can be seen at the locations where the soft sensors are connected to the body modules in Fig. 1.

Each module has a width of 60 mm where motor ends have the length of 25 mm and middle module have the length of 44.5 mm. Motor end module have weight of 15 grams and the middle module has the weight of 10 grams. Overall, the assembled body has the length of 154 mm, the width of 60 mm, the height of 30 mm and a mass of 123 grams.

Similar to the SQuad's design, PDMS is the main material used in M–SQuad's body modules and C-legs. For fabrication, first, the molds necessary for manufacturing the body modules and C-legs are prepared. In total, 3 different types of molds are designed and prepared, one for the middle module, one for the motor, end modules and one for the C-legs. PDMS Sylgard 184 was mixed in a 10:1 ratio of a pre-polymer and cross-linker and mixed for body modules, for the C-legs ratio is kept at 5:1. PDMS is poured into the mold and placed in the oven for 4 hours at 70°C. Then the modules are removed from the mold.

Different from SQuad's C-legs, C-legs used in M-SQuad have an expanded circular width at the locations where the legs are

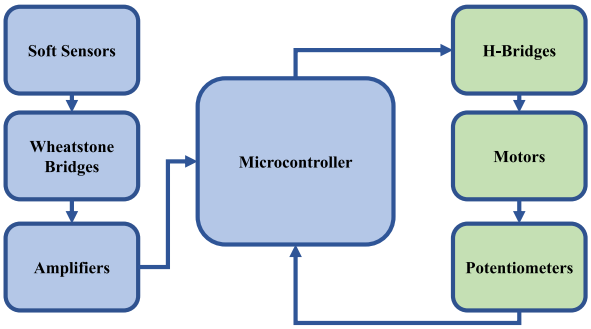

Fig. 3. Architecture of the electronics board of M–SQuad.

attached to the motors in order to raise M–SQuad's body from the ground. These expanded C-legs can be seen in Fig. 1. Raising the robot's body modules was critical to prevent dragging problems. Compared to the SQuad's C-legs, the only significant difference is the expansion of the C-legs.

B. Electronics Design

In the SQuad's circuits, an Arduino Pro Micro and two L293DD H-bridges are used to drive four DC motors. The main components can be summarized with these components. In addition, there are some passive components located on the circuit board in order to prevent any instantaneous voltage fluctuations. Also, a switch and a 3.7-5 V regulator were used on the PCB. M–SQuad also has a similar circuit board architecture.

The electronic design of SQuad differs from M–SQuad mainly because of the four-sensor located on the M–SQuad's body. In order to transmit the responses of these four sensors to the microcontroller, four extra analog read pins are needed. Thus, different from the SQuad, in M–SQuad's circuit board, an Esp-32 was utilized instead of the Arduino Pro Micro because the Esp-32 has more general-purpose input/output pins. Furthermore, unlike Arduino Pro Micro, it has its own embedded Bluetooth module, which is used to transfer the data of the sensors during experiments. Furthermore, for each pair of sensors, an LM358P Op-Amp and two wheat-stone bridges are used on the circuit board.

Wheatstone bridges are used to convert the soft sensor response to a voltage change. The bridges are supplied with 5 V. Wheatstone bridge is formed with 1 kΩ, 3 kΩ, 3.3 kΩ resistors and the actual sensor as the fourth leg. However, the voltage output was very low, and amplification was essential. Thus, for this purpose, LM358P Op-Amps are preferred. Single Op-Amp differential amplifier configuration is used. By using the amplifier circuit, sensor signals are amplified with the desired gain (set to 2.14) by adjusting the resistance with respect to the gain. General architecture of the electronics is shown in Fig. 3.

The designed circuit board is manufactured by a mass manufacturer. Different from SQuad, M–SQuad has a rigid double-sided FR4 PCB. In order to keep the robot body soft, the rigid PCB is placed on the main module, sacrificing this module's compliance but saving the softness of the sensors.

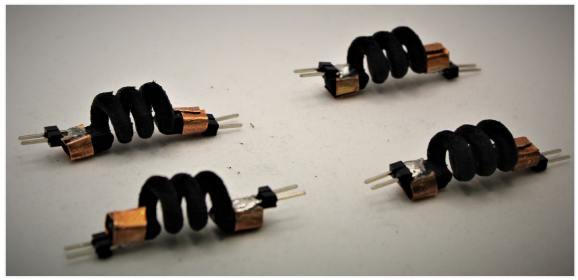

Fig. 4. Soft TPU sensors with copper connections.

C. Sensor Design

The soft sensor is supposed to act both as a structural and as a sensing element for M-SQuad, therefore, there were two critical points for the sensor design. First, the sensor should be stiff and durable enough such that it can connect a pair of modules without the main module sagging all the way to the ground. Additionally, the sensor should be soft enough and should deform considerably so that it is capable of sensing the obstacles and distinguishing the scalable obstacles.

Since the soft nature of M–SQuad will mostly be due to the sensors' compliances, conductive thermoplastic polyurethane was preferred as the main material of the sensors. This is because thermoplastic polyurethane is a flexible material, and it has conductive versions which are available on the market as a 3D printer filament.

In order to determine which sensor geometry is suitable for our case, different geometries were designed and tried such as zigzag shaped, leaf-spring shaped, cantilever shaped, and coil-spring shaped. To understand which geometries perform better for our case, all the geometries are tested separately. All the dimensions of the sensors are kept the same to have a fair comparison between different experiments. The width, length and thickness of the sensors are chosen as 7 mm, 26.4 mm and 3.5 mm respectively. Especially the lengths of the sensors are dictated by the C-leg motion and how close two modules can be placed without the legs hitting each other during locomotion.

Coil-spring shaped sensor, shown in Fig. 4, provides the most clear output compared to other geometries because when the sensor is compressed or bent, the adjacent rings touch each other, and cause a significant resistance decrease. The nominal resistance of the coil-spring shaped sensor is around 3.5-5 kΩ, whereas the other geometry sensors we tried have nominal resistances in the range of 1 kΩ - 2 kΩ. When the other sensors are bent or compressed, resistance decreases in the range of 10%-30%, whereas the resistance of coil-spring shaped sensor decreases 81% under compression or bending.

$$R = \rho L/A, \tag{1}$$

$$\Delta R = \rho/\Delta d_c \tag{2}$$

After coil-spring shaped sensor is selected as the main sensor geometry, we investigated the properties of the sensor. As the sensor is compressed, the coils get closer to each other until eventually they contact and are further compressed into each

TABLE I
MAXIMUM NONLINEARITY AND HYSTERESIS AS PERCENTAGE OF FULL-SCALE-DEFLECTION

	Max. Non-Linearity	Max. Hysteresis
3 coil-spring	13.51%	15.54%
4 coil-spring	19.51%	30.92%

other. We hypothesize that the contact between coils significantly reduces the resistance of the sensor during compression. As more coils contact each other and as the coils are pressed more against each other, the resistance decreases more. This can also be related to (1) where resistance is directly related to the length of the conductor (L) but inversely related to the cross-section area (A).

Equation (1) can be written as (2) where d_c is defined as a characteristic dimension (A/L) and is a function of the sensor's compression amount (x). In (1) and (2), ρ is the constant resistivity of the sensor's material. When the sensor is compressed, the characteristic dimension increases, as a result, the sensor's resistance decreases. However, the function that defines the relation between characteristic dimension dc and the compression amount x is expected to be nonlinear and nonsmooth because the electrical contact between coils forms stochastically due to the electrical break-down phenomenon. A more detailed model of the sensor is planned a future work.

In order to verify the validity of this hypothesis, electrical responses of two different spring sensors (one with three coils and one with four coils) are analyzed on a compression test setup. These two sensors are 3D printed under same conditions and the design parameters such as length, thickness, width and cross-sectional area. Each sensor is examined under 10 mm of compression and decompression. Eight trials are conducted for each sensor response, in total sixteen trials are conducted. Sensor resistance and displacement data are gathered via a data acquisition device with a sampling frequency of 5 kHz. Collected data can be seen in Fig. 5.

The sensor response has three different regions, which we called no coil-contact response, coil-collapsing response, and fully-collapsed response, respectively. These three different regions should be investigated and analyzed separately from each other. A line is fit to each region separately and the line equations are also shown in Fig. 5. These equations can be used to provide a linear estimate for the function between d_c and x. On the other hand, the coil-collapsing response shows nonlinear and non-smooth behavior, which supports our hypothesis of contact between coils significantly affecting the sensor response.

It should also be noted that the nonlinearity of the coil-collapsing regions is more dominant in 4-coils spring sensors compared to 3-coils spring sensors. The maximum nonlinearity and the maximum hysteresis for both sensors as a percentage of full-scale deflection are reported in Table I.

3-coil sensors are preferred for the robot experiments because of their lower max. nonlinearities and max. hysteresis. The sensor has a nominal resistance (resistance without deformation) in the range of 4.2-4.6 kΩ. When the sensor experiences mechanical deformations such as bending, compression, tension

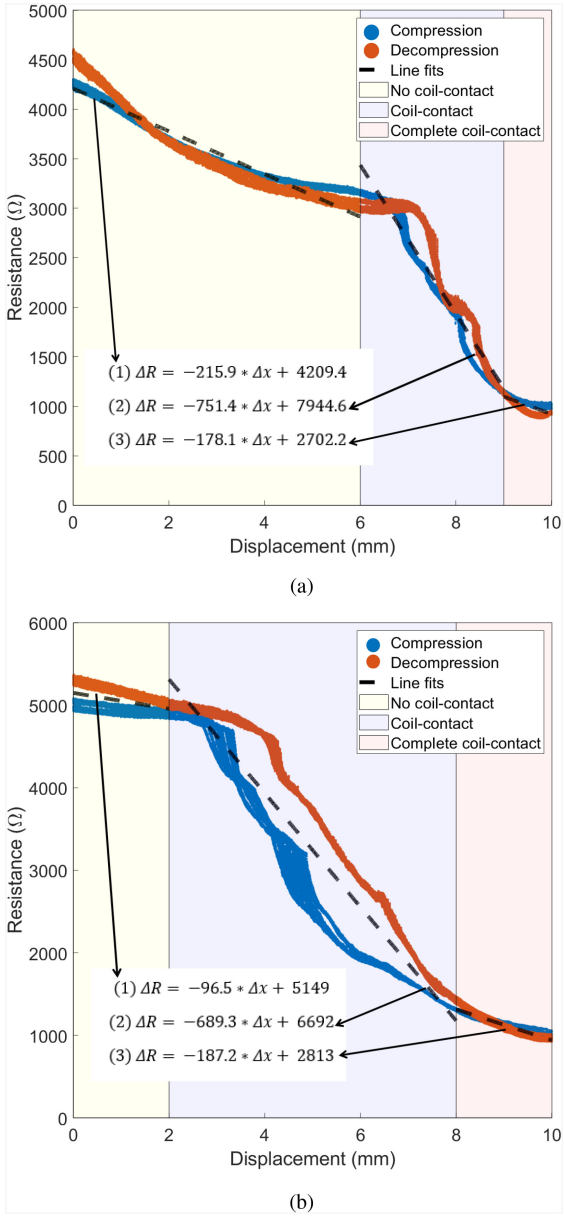

Fig. 5. Resistance change for 10 mm compression of (a) 3 coil-spring shaped sensor (b) 4 coil-spring shaped sensor.

or twist, the resistance of the sensors drops significantly. When the resistance of the sensor drops significantly, the output of the bridge becomes quite large, and when amplified, becomes saturated at 3.3 V since the maximum voltage reading is 3.3 V for our controller board. Relation between the compression amount and the sensor response can be observed from Fig. 6.

Coil-spring shaped sensors are 3D printed using conductive TPU filament with 80% infill. The first layer height is set at 0.27 mm and the other layer heights are kept at 0.18 mm. Nozzle temperature is set to 230°C and the heat bed temperature is set to 65°C. Furthermore, the number of wall perimeter layers is set to one except the top and the bottom layer wall perimeters, which are set to three.

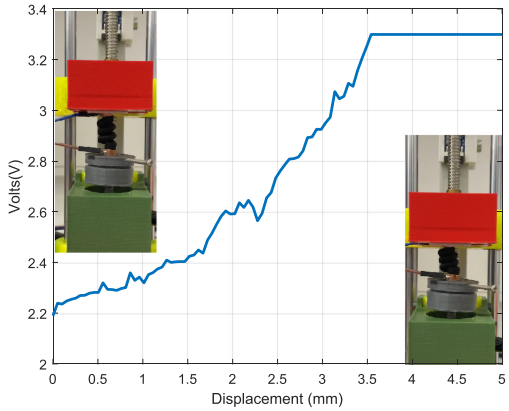

Fig. 6. Compression test of the coil-spring shaped soft sensor.

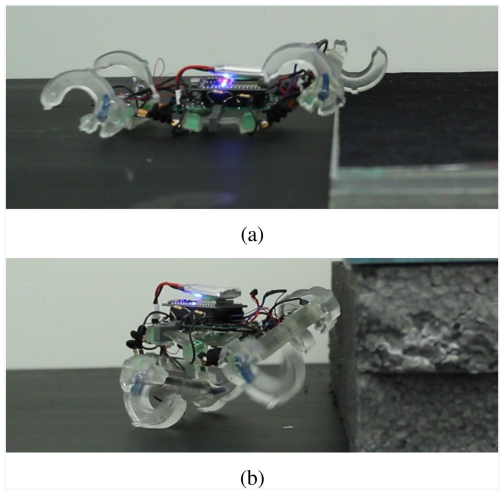

Fig. 7. Photos of M–SQuad when it encounters (a) scalable obstacle (b) non-scalable obstacle.

Coil-spring shaped sensors have extensions at both ends to provide an area for proper electrical and mechanical connection. The connection is achieved with a double male header soldered copper plates as can be observed in Fig. 4. The copper plate is necessary since it is not possible to solder headers to conductive TPU. Male headers are soldered to copper plates before wrapping the copper plates around the sensor extension. In order to prevent connection loss, the copper plate is compressed using pliers. Sensors are then attached to the screw terminals located in the main module and the motor end modules using the double male header located at the sensor ends.

III. Scalable Obstacle Detection

In order to detect whether an obstacle is scalable or not, sensors on the robot are used. Data gained from the soft coil-spring shaped sensors are used and reported as raw data, the data is not filtered in any way. We observed that when the robot hits an obstacle that it cannot scale, sensors on the back of the robot compress until the rings of the spring are touching each other. When this happens, the resistance of the sensors connecting the rear motor end module and the main module drops to a very low resistance value and the measured voltage from the sensors saturate at 3.3 V.

We developed an algorithm so that the robot can respond to obstacles beyond its scaling capabilities. If the sensors on the back of the robot saturate simultaneously and for more than a given threshold of time (selected as one second), the robot understands that it is facing an obstacle that it cannot scale. Then, the robot stops, and the directions of the actuators are reversed so that the robot climbs down and starts to move in the opposite direction.

In Fig. 7(a), the robot encounters with a relatively small obstacle that it can scale. From Fig. 8, we can see that only the rear right sensor readings shown in Fig. 8(d) reach the saturation value and for a very short duration. The rear left sensor reading shown in Fig. 8(c) reaches to a high value, yet does not saturate. Such a sensor response is typical during climbing over scalable obstacles.

In Fig. 7(b), robot encounters an obstacle that it cannot scale. In Fig. 9(c) and (d), we can observe that, while the robot tries to climb the obstacle, there are first small peaks for a short duration

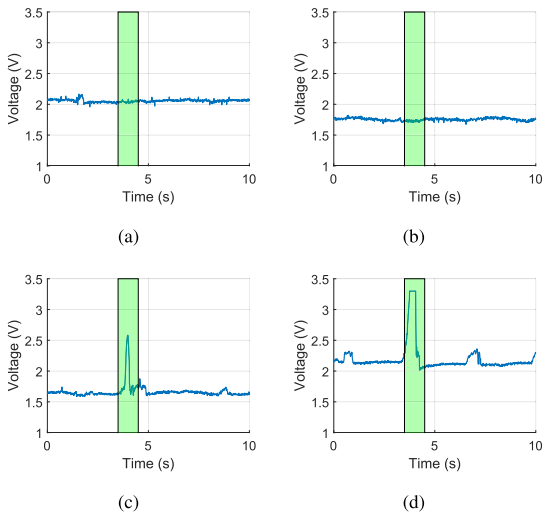

Fig. 8. The data obtained from the sensors, when M–SQuad hits a scalable obstacle: (a) front left sensor, (b) front right sensor, (c) rear left sensor, (d) rear right sensor.

at first. Eventually, when the front of the robot starts to climb and the robot bends significantly, the readings from the rear sensors saturate for a significant time. So, the robot evaluates this as trying to climb over an unscalable obstacle, stops and moves backward.

In order to evaluate the reliability of robot's decision-making (if an obstacle is scalable or not) twenty-six trials are conducted with a relatively small obstacle that the robot is expected to scale easily. In only one of the twenty-six trials, M-SQuad failed to identify the obstacle as scalable. However, after investigating the video footage of the experiment, we observed that the tip of the sensor terminal was stuck on the obstacle while scaling and the robot got stuck. This caused the sensors to get compressed more than the threshold and the robot labeled the obstacle unscalable. Even though, this was a valid concern for the robot, and if continued the robot might have gotten broken, we considered this case to be a failure. After twenty-six trials, the success rate

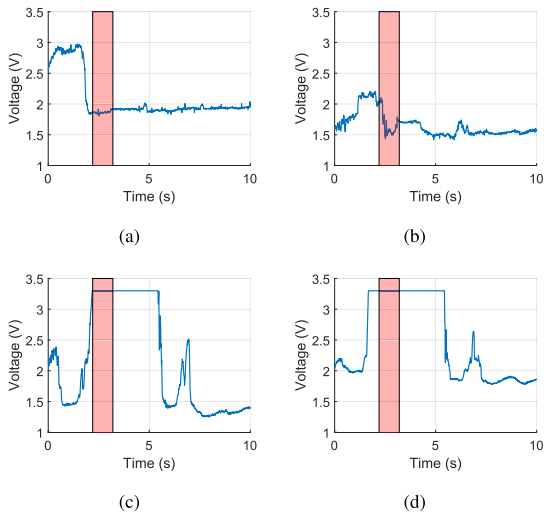

Fig. 9. The data obtained from the sensors, when M–SQuad hits a non-scalable obstacle: (a) front left sensor, (b) front right sensor, (c) rear left sensor, (d) rear right sensor.

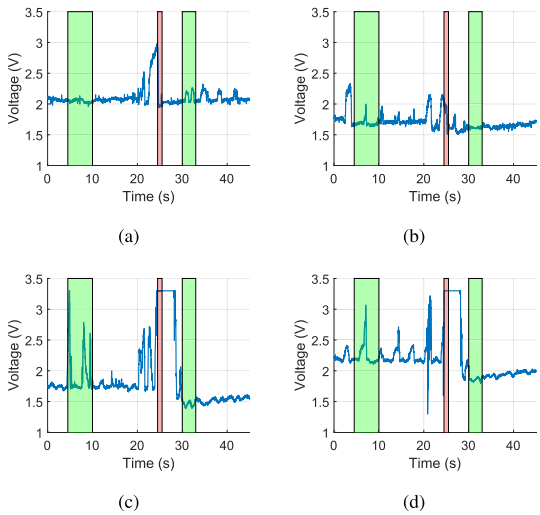

Fig. 10. The sensor data obtained from the sensors during the case study. M–SQuad first it hits scalable obstacle, then nonscalable obstacle, return and hit the scalable obstacle again. (a) Front left sensor, (b) front right sensor, (c) rear left sensor, (d) rear right sensor.

of distinguishing the scalable obstacle is higher than 96% (25 out of 26).

Additionally, we conducted twenty-seven trials with an obstacle that the robot cannot scale. In total, the robot labeled the obstacle as not scalable correctly with a success rate of higher than 92% (25 out of 27). In each trial, the time elapsed during detection was gathered from the videos. The average time between obstacle contact and decision-making is found as 3.81 seconds, with a standard deviation of 1.56 seconds.

IV. Case Study

To demonstrate the scalable obstacle detection capabilities of the robot, a simple parkour is prepared. We placed two obstacles back-to-back, where the first obstacle is 20 mm in height and the second one is around 150 mm, which is much higher than M-SQuad can climb over. The robot was expected to detect and pass the first obstacle, detect the second obstacle as non-scalable, move backward and scale the first obstacle again.

Fig. 10 illustrates the data obtained from the soft sensors on the robot during the demonstration. Green sections represent successful obstacle scaling of the robot, while the red sections represent where the robot fails to scale the obstacle and reverse the moving direction. The first green section shows where robot encounters the first obstacle and Fig. 11(a) shows a screenshot from the video of the experiment. It can be seen in the first green section in Fig. 10(c) and (d) that sensor readings reach a peak value instantaneously during the climbing, the time threshold is not exceeded before the sensor levels drop, so robot continues the mission. After that, robot encounters the second obstacle, for which a screenshot is shown in Fig. 11(b), and fails to scale it. Red section in the Fig. 10(c) and (d) shows the one-second period of saturated reading of the rear sensors. As the saturated readings from the rear sensors exceed one-second duration, robot waits for another second and reverses the directions of the motors to move backward. While moving backward, robot encounters the

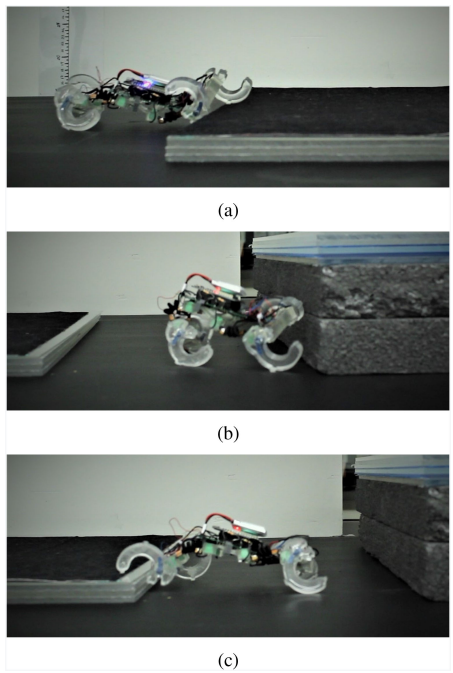

Fig. 11. Photos from case study video when M–SQuad hits the (a) scalable obstacle while moving forward, (b) non-scalable obstacle, (c) scalable obstacle while moving backward.

first obstacle again, which is illustrated by the second green section for the rear sensors in Fig. 10(c) and (d). However, this time as the robot is moving backward, front sensors are the focus of interest for detecting the obstacles and there are no significant changes in the sensor readings as can be seen in Fig. 10(a) and (b). As a result, the robot continues to move in the same direction. The moment that the robot encounters the scalable obstacle while moving backward is shown in Fig. 11(c). It should also be noted here that the locomotion of the robot in the forward direction and reverse direction may differ from

each other in trot gait because of the C-shaped legs used in the M-SQuad design. Therefore, it is expected to see different sensor behaviors, however, it is not a significant difference since the sensors still can detect the obstacles and distinguish them as scalable or non-scalable. Our experiments and the case study can be seen in the video submitted as a supplementary material to this paper.

V. Conclusion and Future Work

In this work, a new version of our untethered miniature soft quadruped is introduced. M–SQuad consists of three modules, which are connected to each other by soft sensors. These sensors are serving as sensing elements and structural elements that connect modules to each other. During the locomotion of the robot, the body deforms, thus, sensors deform as well. Therefore, the resistance of the sensors changes. Obstacles can be both detected and distinguished as scalable or not scalable using these sensors and obstacle detection algorithm. In the case study, it can be observed that the robot can accomplish to detect and distinguish the obstacles that it can climb or not. To the best of our knowledge, this is one of the first times soft sensors are used for environmental detection in mobile robots in literature.

As the future works, the sensor characterization will be improved and the sensor model will be constructed in detail, in order to investigate the possibility of using this sensor for gait control or any other environmental effect detection like incline or roughness of the ground that the robot walks on. The main motivation for the future is to replace the hard encoders with these soft sensors to be one step closer to a soft quadruped with no rigid components.

Acknowledgment

The authors would like to thank Haider Raheem, Muhammed Ali Khan and members of Bilkent Miniature Robotics Laboratory for their invaluable assistance throughout this project.

References

[1] D. Drotman, S. Jadhav, M. Karimi, P. de Zonia, and M. T. Tolley, "3D printed soft actuators for a legged robot capable of navigating unstructured terrain," in *Proc. IEEE Int. Conf. Robot. Automat.*, 2017, pp. 5532–5538.

[2] S. Kim, C. Laschi, and B. Trimmer, "Soft robotics: A bioinspired evolution in robotics," *Trends Biotechnol.*, vol. 31, no. 5, pp. 287–294, 2013. [Online]. Available: https://www.sciencedirect.com/science/article/pii/S0167779913000632

[3] C. Laschi and B. Mazzolai, "Lessons from animals and plants: The symbiosis of morphological computation and soft robotics," *IEEE Robot. Automat. Mag.*, vol. 23, no. 3, pp. 107–114, Sep. 2016.

[4] M. S. Xavier, A. J. Fleming, and Y. K. Yong, "Experimental characterisation of hydraulic fiber-reinforced soft actuators for worm-like robots," in *Proc. 7th Int. Conf. Control, Mechatronics Automat.*, 2019, pp. 204–209.

[5] J. Tao *et al.*, "Triboelectric nanogenerator sensors for soft robotics aiming at digital twin applications," *Nature Commun.*, vol. 11, Oct. 2020, Art. no. 5381.

[6] J. Walker *et al.*, "Soft robotics: A review of recent developments of pneumatic soft actuators," *Actuators*, vol. 9, no. 1, 2020. [Online]. Available: https://www.mdpi.com/2076-0825/9/1/3

[7] D. Rus and M. Tolley, "Design, fabrication and control of soft robots," *Nature*, vol. 521, pp. 467–75, May 2015.

[8] M. Wehner *et al.*, "An integrated design and fabrication strategy for entirely soft, autonomous robots," *Nature*, vol. 536, no. 7617, pp. 451–455, Aug. 2016. [Online]. Available: https://doi.org/10.1038/nature19100

[9] T. G. Thuruthel, B. Shih, C. Laschi, and M. T. Tolley, "Soft robot perception using embedded soft sensors and recurrent neural networks," *Sci. Robot.*, vol. 4, no. 26, 2019, Art. no. eaav1488.

[10] B. Shih *et al.*, "Design considerations for 3D printed, soft, multimaterial resistive sensors for soft robotics," *Front. Robot. AI*, vol. 6, 2019, Art. no. 30. [Online]. Available: https://www.frontiersin.org/article/10.3389/frobt.2019.00030

[11] T. G. Thuruthel, B. Shih, C. Laschi, and M. T. Tolley, "Soft robot perception using embedded soft sensors and recurrent neural networks," *Sci. Robot.*, vol. 4, no. 26, 2019, Art. no. eaav1488. [Online]. Available: https://www.science.org/doi/abs/10.1126/scirobotics.aav1488

[12] K. B. Justus *et al.*, "A biosensing soft robot: Autonomous parsing of chemical signals through integrated organic and inorganic interfaces," *Sci. Robot.*, vol. 4, no. 31, 2019, Art. no. eaax0765.

[13] A. Atalay *et al.*, "Batch fabrication of customizable silicone-textile composite capacitive strain sensors for human motion tracking," *Adv. Mater. Technol.*, vol. 2, no. 9, 2017, Art. no. 1700136. [Online]. Available: https://onlinelibrary.wiley.com/doi/abs/10.1002/admt.201700136

[14] Y. Mengüç *et al.*, "Wearable soft sensing suit for human gait measurement," *Int. J. Robot. Res.*, vol. 33, no. 14, pp. 1748–1764, 2014.

[15] B. Shih *et al.*, "Electronic skins and machine learning for intelligent soft robots," *Sci. Robot.*, vol. 5, no. 41, 2020, Art. no. eaaz9239.

[16] Y. Xu *et al.*, "A flexible multimodal sole sensor for legged robot sensing complex ground information during locomotion," *Sensors*, vol. 21, no. 16, 2021, Art. no. 5359. [Online]. Available: https://www.mdpi.com/1424-8220/21/16/5359

[17] W.-Y. Li, A. Takata, H. Nabae, G. Endo, and K. Suzumori, "Shape recognition of a tensegrity with soft sensor threads and artificial muscles using a recurrent neural network," *IEEE Robot. Automat. Lett.*, vol. 6, no. 4, pp. 6228–6234, Oct. 2021.

[18] M. A. I. Kalın, C. Aygul, A. Turkmen, J. Kwiczak-Yigitbasi, B. Baytekin, and O. Ozcan, "Design, fabrication, and locomotion analysis of an untethered miniature soft quadruped, squad," *IEEE Robot. Automat. Lett.*, vol. 5, no. 3, pp. 3854–3860, Jul. 2020.

[19] N. Mahkam, T. B. Yılmaz, and O. Özcan, "Smooth and inclined surface locomotion and obstacle scaling of a C-legged miniature modular robot," in *Proc. IEEE 4th Int. Conf. Soft Robot.*, 2021, pp. 9–14.